Development of a microfurnace dedicated to in situ scanning electron microscope observation up to 1300 °C. I. Concept, fabrication, and validation

Jérôme Mendonça, Henri-Pierre Brau, Dorian Nogues, Antoine Candeias, Renaud Podor

Development of a microfurnace dedicated to *in situ* Scanning Electron Microscope observation up to 1300°C - Part I: Concept, fabrication and validation

Jérôme MENDONÇA [1,2], Henri-Pierre BRAU [1], Dorian NOGUES [2], Antoine CANDEIAS [2], Renaud PODOR[1]*

[1]ICSM, Univ Montpellier, CNRS, CEA, ENSCM, Bagnols-sur-Cèze, France

[2]NewTec Scientific, 2 route de Sommières, 30820 CAVEIRAC

* Corresponding author

e-mail: renaud.podor@cea.fr

Tel: 00 (33) 04.66.33.92.02

Mailing addresses:

Dr Jérôme MENDONÇA

NewTec Scientific

2 route de Sommières

30820 CAVEIRAC

FRANCE

Henri-Pierre BRAU

Institut de Chimie Séparative de Marcoule

Site de Marcoule, Bâtiment 426

BP 17171

F-30207 Bagnols sur Cèze Cedex

France

Dorian NOGUES

NewTec Scientific

2 route de Sommières

30820 CAVEIRAC

FRANCE

Antoine CANDEIAS

NewTec Scientific

2 route de Sommières

30820 CAVEIRAC

FRANCE

Renaud PODOR

Institut de Chimie Séparative de Marcoule

Site de Marcoule, Bâtiment 426

BP 17171

F-30207 Bagnols sur Cèze Cedex

France

Abstract: The development of a new heating system dedicated to *in situ* scanning electron microscope (SEM) experimentation at high temperature is reported. This system, called FurnaSEM, is a compact microfurnace enabling heat treatments up to 1300°C. The choice of materials for the microfurnace is explained. The design of the microfurnace is optimized by iterations of numerical simulations, and the thermal characteristics of the microfurnace are calculated numerically. The numerical results obtained are compared with the thermal characteristics of a manufactured microfurnace, measured on a specially developed dedicated test bench. This test bench includes a working chamber simulating a SEM chamber equipped with a thermal camera. The results obtained during various qualification tests enabled us to determine the main technical characteristics of the FurnaSEM microfurnace: temperature profiles on the sample support surface, energy consumption at high temperature and the range of achievable thermal cycles.

Keywords: SEM, furnace, *in situ*, high temperature, modeling

1. Introduction

The *in situ* study of material behavior during heat treatment is a key approach to a detailed understanding of their reactions and transformations under service conditions, which can be addressed by various analytical techniques [1,2,3,4,5,6]. To achieve this, it is often necessary to develop specific heating devices adapted to the requirements [7,8,9,10]. Today, the observation of materials on a micro/nanometric scale under various chemical (humidity, presence of gas) or physical (mechanical load or heat flux) constraints can be achieved with the aid of electron microscopy, in particular scanning electron microscopy (SEM) [11,12,13].

Since the 1960s, mini-heating devices have been developed for use in conventional or environmental SEMs. Coupling the SEM with a microfurnace is a particularly interesting analytical tool for characterizing the behavior of materials at the micrometer scale, and in some cases at the nanometer scale, over a wide temperature range (from RT to 1000°C) [14,15,16,17,18,19], and in special cases up to 1500°C [20,21,22,23,24]. Numerous works covering various disciplinary fields using this technique are reported in the literature. Experiments have been carried out in a wide range of environments, from high vacuum to low vacuum, using a wide variety of gases [25,26,27,28]. These experiments are generally described as "*in situ*", "high temperature SEM" or "HT-SEM". The terms "environmental" and "variable pressure" modes appear in experiments carried out with partial gas pressure, thus qualifying the framework in which the observations are made [29]. The main advantage of performing *in situ* experiments in the SEM is to use samples with dimensions representative of a bulk material [30,31,32,33,34]. A sample of a few mm^3 can be placed on a dedicated heating plate, making it possible to visualize a surface area of some mm^2 using electronic imaging. In this way, the observations provide a clear picture of the behavior of a solid material under operating conditions [35]

The HT-SEM technique can suffer from technical limitations inherent in heating materials to high temperatures, which can make image recording difficult. One of the difficulties generally reported concerns thermionic emission (or thermo-emission) from hot elements present in the SEM chamber. Surfaces heated to high temperatures emit thermal electrons, which contribute to the electronic signals collected for image formation. At high temperatures, thermionic emission leads to an attenuation of the secondary electronic signal, requiring complex adjustments when the working temperature exceeds around 1050°C [36,37]. The intensity of thermionic emission can be estimated from the Richardson-Dushman law, which relates emission current density to temperature according to the relationship [38]:

$$j = A_0 \times C_f \times T^2 \times \exp\left(\frac{-\psi}{k_b T}\right) \quad (1)$$

Where j is the electronic current density, $A_0 = \frac{4\pi \times m \times e \times k_b^2}{h^3}$ is a parameter formulated from the physical constants: m is the mass of an electron, e the electric charge of an electron, k_b Boltzmann's constant and h Planck's constant. C_f is a material-dependent correction factor, ψ is the work function of an electron in vacuum (i.e. potential barrier to let an electron escape from the surface of a material into vacuum) and T the temperature of the emissive material. When $k_b T \gg |\psi|$ then $j \propto T^2$. Thermionic emission increases rapidly with temperature.

However, thermionic emission is not the only source of image disturbance when a sample is heated. Black body thermal emission - present even in a vacuum and predominant at high temperatures - produces heat mainly in the infrared (IR) domain. This radiation can heat up the components in the microscope chamber (detectors, sample holders, objective lens, etc.). The closer these components are to the emitting source, the more intense the heating. Thus, if the microscope chamber is cramped, this radiation can potentially damage the microscope. However, the ability of surfaces exposed to the radiation to absorb IR light also plays a significant role. Reflective surfaces such as polished metal surfaces can limit the heating effect. In general, small components close to the hot source, such as SEM detectors, are the most exposed to the risk of overheating. At the same time, thermal emission produces intense illumination that scrambles the signal from photosensitive elements such as the photocathodes used in detector photomultipliers. The saturation of these elements by visible light makes it impossible to use them for high-temperature image acquisition. This is the case with conventional backscattered electron detectors or diodes for X-ray photon collection. Special detectors have been developed to make image acquisition accessible even at high temperatures [39,40,41]. The intensity of thermal radiation emitted by a surface is related to temperature by Stefan-Boltzmann's law:

$$Q_{rad} = \varepsilon \times S_{rad} \times T^4 \quad (2)$$

Where Q_{rad} is the radiated heat flux, ε is the total emissivity of the emissive material and S_{rad} is the radiating surface area. Like thermionic emission, thermal radiation strongly increases with temperature.

Other phenomena - generally thermo-activated - can make *in situ* SEM experiments at high temperatures more difficult. Traces of volatile compounds or pollutants adsorbed on surfaces can be released into the chamber when these surfaces are heated, particularly in high vacuum mode. If the outgassing flow is too high in comparison with the pumping rate, pollutants may be concentrated in the sample environment, contaminating the surface. This contamination can also lead to rapid degradation of the furnace heating element if it is made of a material that is potentially reactive at high temperatures. On the other hand, *in situ* temperature

experiments in the SEM to observe chemical reactivity lead to the use of tools that can be implemented in all types of atmospheres. The use of hot gases (oxidizing, reducing, nitriding, fuel, etc.) can also lead to a rapid degradation of the heating system if the materials used are not appropriate.

The aim of this work is to develop a new microfurnace dedicated to *in situ* experiments in the SEM called "FurnaSEM", whose configuration will take into account all these constraints and guarantee both its integrity during the experiment and its neutrality in relation to the working environment (no outgassing). All the above points have been taken into account in the design of this microfurnace, in order to propose a system that is compact, stable and easy to set up for *in situ* SEM observations up to a temperature as high as 1300°C.

In this first article in a series dedicated to the development of the FurnaSEM microfurnace, we describe the design of the microfurnace based on a numerical model. This approach makes it possible to establish numerical temperature maps and identify furnace design defects without having to build the furnace [23,24,42]. We will present the physical criteria adopted to select the materials used for its manufacture, and report on the performance validation tests of the FurnaSEM microfurnace built on the basis of the optimization of the numerical model. Validation of the performance of the actual device built and determination of its technical characteristics will be obtained by implementing a test bench developed and built specifically for this study. In the second article of the series, we will focus on qualifying the thermal behavior of a sample when placed in the hot zone of the furnace. Finally, in the third article, we will report on experiments carried out *in situ* at high temperature in the microscope chamber, to assess the actual behavior of the furnace and the new imaging possibilities that open up to researchers.

2. FurnaSEM microfurnace design

2.1. Selection criteria and selected design

The first choice is to use a Joule-heating system, for reasons of universality of operation and relative ease of control of furnace and sample temperature, during temperature ramps and isothermal heating. Other technical solutions such as direct sample heating with the Joule-effect, by passing current through the sample itself, or laser heating are sometimes used to develop miniature devices [42,43,44,45]. Direct sample heating was not selected as it is not universal, as insulating materials cannot be heated using this technique, nor can powder materials. Laser heating can make it difficult to control sample temperature and achieve uniform heating of relatively large samples. It can also generate stray reflections in the SEM chamber. Consequently, although laser heating can offer the advantage of achieving very rapid

temperature ramps (in heating and cooling) and access to very high sample temperatures [12, 14,46,47], this solution was not retained to develop the FurnaSEM microfurnace.

The FurnaSEM microfurnace has been designed with the aim of producing an instrument that can operate under a wide range of the most severe experimental conditions (i.e. high-temperature heating in the presence of gas). To achieve this, the architecture of the microfurnace has been designed to limit the disturbing sources mentioned above. The device must satisfy specific physico-chemical properties that have been taken as selection criteria. These criteria are grouped into "thermal", "mechanical" and "chemical" categories, and are presented in **Table 1**. The values required for each of the selection criteria are very demanding, and place a strong limit on the structural materials that can potentially be used to design the microfurnace. The best compromise is found in the family of metal alloys that offer high mechanical strength at high temperatures, can be shaped by conventional machining processes, and are insensitive to the presence of oxidizing, neutral or reducing gases.

Table 1 - Summary of the characteristics used as selection criteria for the FurnaSEM heating system. The required values are given qualitatively to show their influence clearly.

Category	Property	Expected values	Influence
Thermal	Thermal conductivity	High	Temperature homogeneity
	Volumetric heat capacity	Low	Thermal inertia
	Emissivity	Low	Radiated stray heat
Mechanical	Melting temperature	High	High-temperature integrity
	Coefficient of thermal expansion (CTE)	Low	Mechanical distortion and electronic image drift
	Creep strength	High	Durability at high temperatures
Chemical	Resistance to oxidation and other forms of corrosion	High	Compatible with environmental SEM
	Thermal emission	Low	Scrambling of electronic images
	Vapor pressure	Low	Vacuum outgassing rate

Few materials meet these criteria. A platinum-based alloy with a low rhodium content (<5%wt) was chosen to manufacture the hot sample holder. This alloy offers overall characteristics that are most in line with the selected criteria. It combines good thermal

properties with good chemical stability in oxidizing atmospheres such as ambient air at residual pressure. The physical characteristics of this alloy are reported in **Table 2**.

Table 2 - Physical properties considered for a Pt-x%Rh ($0 \leq x \leq 10$) alloy chosen to manufacture the FurnaSEM microfurnace over the 20-1300°C temperature range. Most properties correspond to those of pure platinum.

Properties	Symbol [unit]	Range of values from RT to 1300°C	Reference
Melting temperature	$T_{melting}$ [°C]	1800 - 1830	[48]
Thermal conductivity	k [$W.m^{-1}.K^{-1}$]	70 - 85	[49]
Volumetric heat capacity	ρ.Cp [$kJ.m^{-3}.K^{-1}$]	2815 - 3595	[50]
Total emissivity	ε [-]	0.05 - 0.19	[51]
Coefficient of linear thermal expansion (CLTE)	α_{th} [$10^{-6}.K^{-1}$]	9.04 - 13.3	[52]
Vapor pressure	p_{vap} [Pa]	$5.38.10^{-6}$ [at 1300°C]	[53]
Electronic Work function	ψ [eV]	5.12 - 5.93	[54]

The heating element consists of a mineral-insulated platinum-rhodium alloy heating element shaped into a spiral and welded to the underside of the sample holder, also made of platinum-rhodium alloy. The heating element is heated by joule effect. Its maximal admissible temperature is around 1400°C given the heating element's small dimensions and structure. The sample holder welded to the resistive filament forms the hot zone of the microfurnace. It is designed to be connected to the cooled external part of the microfurnace. The optimized design, obtained after several iterations of the numerical model, is shown in three-dimensions on the **Figure 1**.

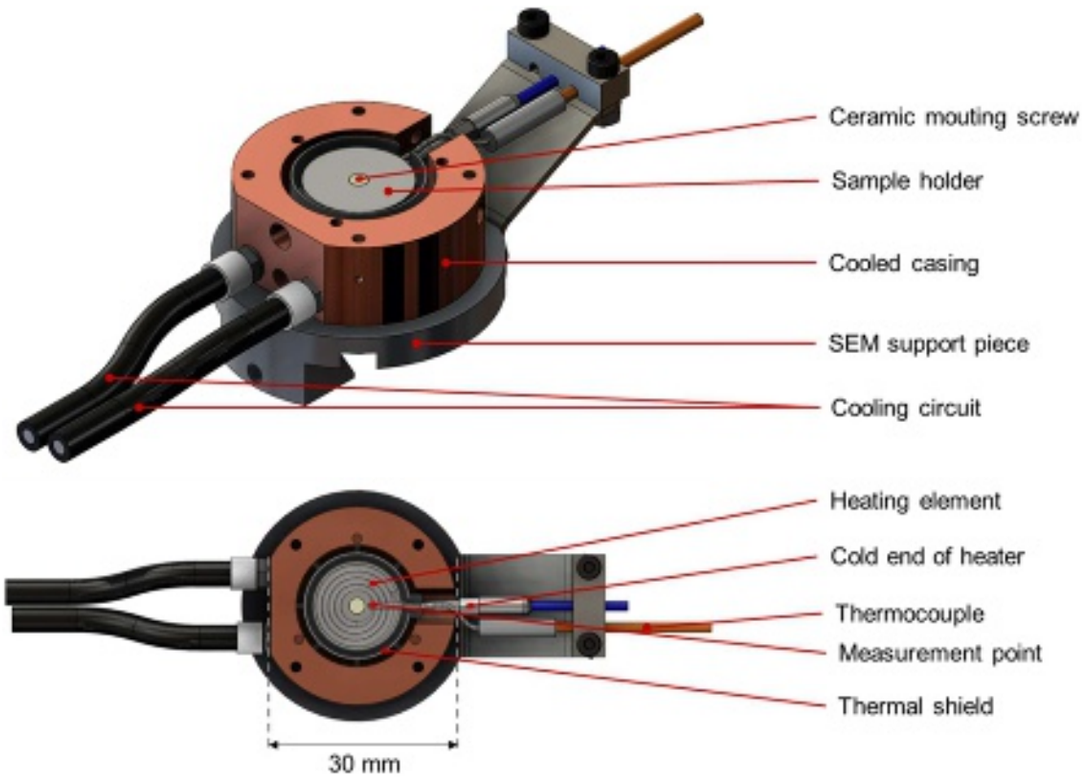

Figure 1 - 3D and surface views of the FurnaSEM microfurnace for *in situ* heat treatment up to 1400°C.

The FurnaSEM hot-stage is a compact, cylinder-shaped heating device. The hot part of the microfurnace is mounted in such a way that it has minimal contact with the rest of the furnace. This so-called floating assembly is achieved by holding the heating element to the furnace body only by means of an insulating ceramic screw, thus minimizing heat loss to the microfurnace housing. Heat shields with polished surfaces surround the sample holder (excluding the side facing the electron beam) to block high-temperature heat radiation. An additional shield can be installed on the working part of the furnace to reinforce thermal insulation (this shield is not shown in **Figure 1**). The external part of the microfurnace consists of a housing cooled by circulating water and mounted on a SEM-compatible interface. This housing acts as a heat sink, limiting heating of the external parts of the furnace. Temperature is measured by inserting a thermocouple as close as possible to the surface of the sample holder. The main structure of the furnace has a diameter of around 30 mm. These limited dimensions make the microfurnace easy to implement in most SEMs.

2.2. Determination of thermal performance of the microfurnace by numerical simulation

To determine the thermal performances of the FurnaSEM microfurnace, heat transfers simulations within the furnace, and between the furnace and its environment, were carried out

using Flow Simulation©, a commercial software package integrated into the SolidWorks© software suite (Dassault system). This software simulates the 3 modes of heat transfer (conduction, convection and radiation) through numerical discretization using the finite volume method. A brief description of the physical models used in the software is given in supplementary information **SI-1**. Physical modeling was used to optimize the FurnaSEM microfurnace design. Important points considered in optimizing the furnace geometry were the verification of the temperature field on the surface on which the samples are placed, and the minimization of the heating power required to reach a temperature of 1300°C. The virtual model of the optimized microfurnace (**Figure 1**) is used to model the thermal behavior of the system under defined conditions (specified below). The software's capabilities make it possible to model heating under high vacuum conditions and - to a lesser extent - under low-vacuum conditions by simulating the convective flow of the residual atmosphere around the furnace (see **SI-1** for more details). To cover a wide range of system operating conditions, simulations were carried out for two vacuum levels:

- High vacuum (HV) mode (i.e. less than 10^{-3} Pa), where only conduction and radiation are solved
- Low vacuum (LV) mode where natural convection is added with a residual air pressure of 300 Pa.

Numerical simulations are carried out in steady state on a calculation grid of around 310,000 solid meshes (FurnaSEM solid parts) and 3,400 fluid meshes (cooling circuit). In the case of LV mode calculations, 126,000 meshes are added to account for external gas flow around the furnace. The various physical conditions implemented for the calculations are summarized in **Table 3**.

Table 3 - Physical conditions used for numerical calculations to simulate FurnaSEM microfurnace behavior. Reminder of the main material properties used for these calculations.

Heat transfer	**High vacuum (HV)**	**Low vacuum (LV)**
Conduction	Yes	Yes
Convection	No	Yes (air at 300 Pa)
Radiation	Yes	Yes

Boundary conditions	**High vacuum (HV)**	**Low vacuum (LV)**

Heating element power range: Q_{heat} **[W]**	1 - 50
Cooling flow rate: q_v **[mL/min]**	120
Room temperature: T_{room} **[°C]**	20

Material thermal properties	**High vacuum (HV)**	**Low vacuum (LV)**
Platinum thermal conductivity: k_{Pt} **[W/m.K]**	70 - 85 (20 to 1300°C)	
Platinum emissivity: ε_{Pt}	0.1 – 0.2 (20 to 1300°C)	
Copper thermal conductivity: k_{Cu} **[W/m.K]**	400 (15 to 30 °C)	
SS 304L thermal conductivity: k_{SS304L} **[W/m.K]**	14.78 – 27.43 (20 to 1300°C)	
SS 304 L emissivity: ε_{SS304L}	0.26 – 0.29 (20 to 1300°C)	

The results obtained for a heating power of around 40 W, in high vacuum mode, are shown in **Figure 2a**. FurnaSEM's global temperature field shows that heat remains confined to the central part of the furnace (hot zone) as expected. The cooling circuit is sufficiently efficient to maintain the outer shell of the microfurnace at ambient temperature. Heat leakage is observed towards the cable support parts (heating element and thermocouple) where a maximum temperature of around 200°C is expected. This heat leakage cannot be avoided, as these parts support the cold termination of the heating element (whose temperature tends towards 500°C when heating to close to 1300°C). A maximum local temperature of 1300°C (thermocouple measurement point) is obtained under these conditions. Results obtained with LV mode conditions are depicted in terms of furnace rating power in **Figure 2b**. The required power to reach a given temperature is significantly higher in LV mode than in HV mode as expected. Convection heat loss induce an additional energy consumption about 40 – 100% (depending on the target temperature) relatively to the HV mode.

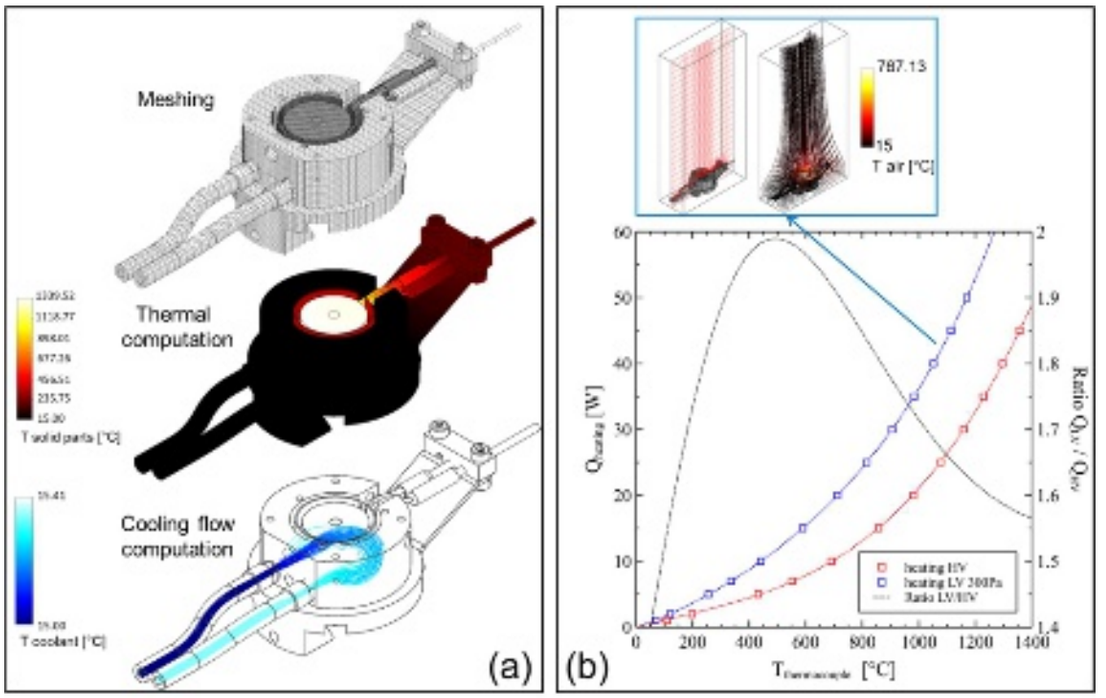

Figure 2 - Numerical simulations of FurnaSEM microfurnace thermal characteristics. (a) Furnace mesh and temperature profiles obtained for 40W heating power in high-vacuum mode. (b) Power-temperature relationship at the thermocouple point for the two vacuum levels considered. Modeled gas flow around the furnace is shown at top right.

The temperature field on the sample surface was also determined for all simulation conditions. The thermal profiles of this region need to be as uniform as possible to ensure a homogeneous sample heating. According to the results of the numerical simulations obtained (**Figure 3**) the temperature field at the surface of the hot zone shows limited temperature dispersion around the mean value. At high heating power (i.e. 40 – 50 W), local temperature differences on the hot zone do not exceed 20°C despite the high working temperature (1200 and 1350°C respectively). On the other hand, the residual temperature heterogeneities all have the same characteristics, namely a systematic hot-cold disparity that can be seen from left to right on the thermal fluctuations maps (**Figure 3a** and **Figure 3c**). The coldest region is where the thermocouple and heater termination are located, acting as heat sinks. The temperature sensor disturbs the whole system, as its presence creates a thermal leakage point that lowers the local temperature at the point of measurement. This is confirmed by the data plotted in **Figure 3b** and **Figure 3d** where local temperatures at the thermocouple position are lower than the mean surface temperature. The deviation is between 2 and 3 standard deviations (i.e. labelled as ± 2σ and ± 3σ in the figure), depending on the conditions simulated. Similarly, the cold part of the heating element causes a localized lowering of heat source, leading to local

cooling (blue zone in the figures). Hot-cold disparities have a maximum magnitude of around 25°C when the average surface temperature of the hot zone exceeds 1400°C. Switching from high vacuum mode to low vacuum mode does not modify these trends.

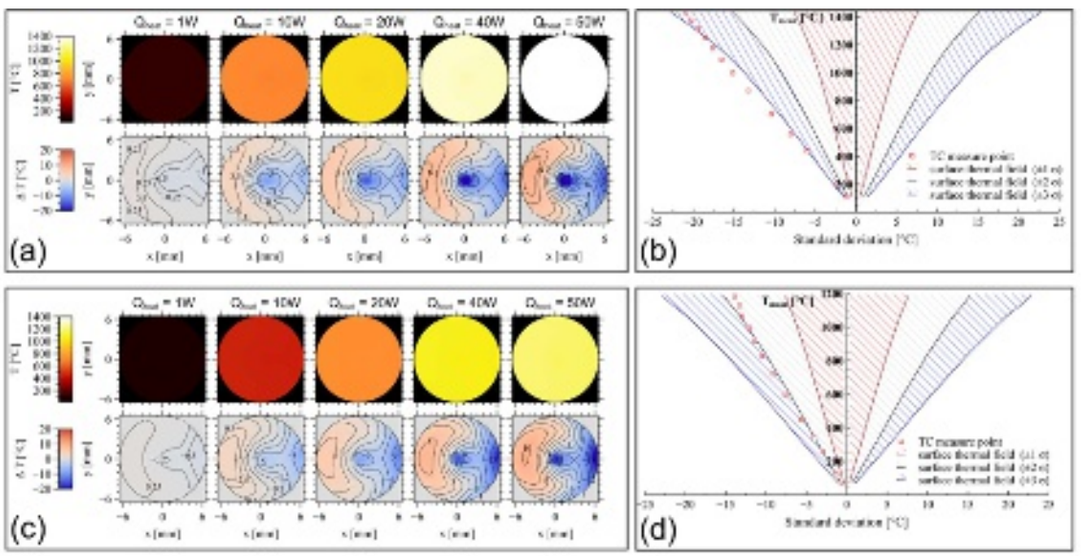

Figure 3 - Simulated temperature profiles of the sample holder surface as a function of heating power input. (a) Heat maps and thermal fluctuation maps for high vacuum mode. (b) Deviation from the mean temperature of the thermocouple measurement associated with the profiles. (c) Heat maps and thermal fluctuations maps for low vacuum mode. (d) Deviation from the mean temperature of the thermocouple measurement associated with the profiles.

The FurnaSEM device architecture, as obtained after optimization of the thermal characteristics, leads to a set of results that allow us to predict that the targeted thermal characteristics of the furnace (i.e. 1300°C) can be achieved. These data will be consolidated by an experimental approach in which a manufactured microfurnace will be tested under conditions representative of the SEM operating mode.

3. Characterization of microfurnace performance under controlled conditions

A FurnaSEM microfurnace was built in accordance with the design and materials selected. The resulting device is shown in **Figure 4**. The furnace is connected to a controller positioned outside the work chamber for power supply. A sealed passageway between the test chamber and the outside allows electrical and hydraulic circuits to pass from the furnace to the control unit. The furnace is equipped with an S-type thermocouple lined with a Pt90/Rh10 sheath capable of resisting oxidation at high temperatures.

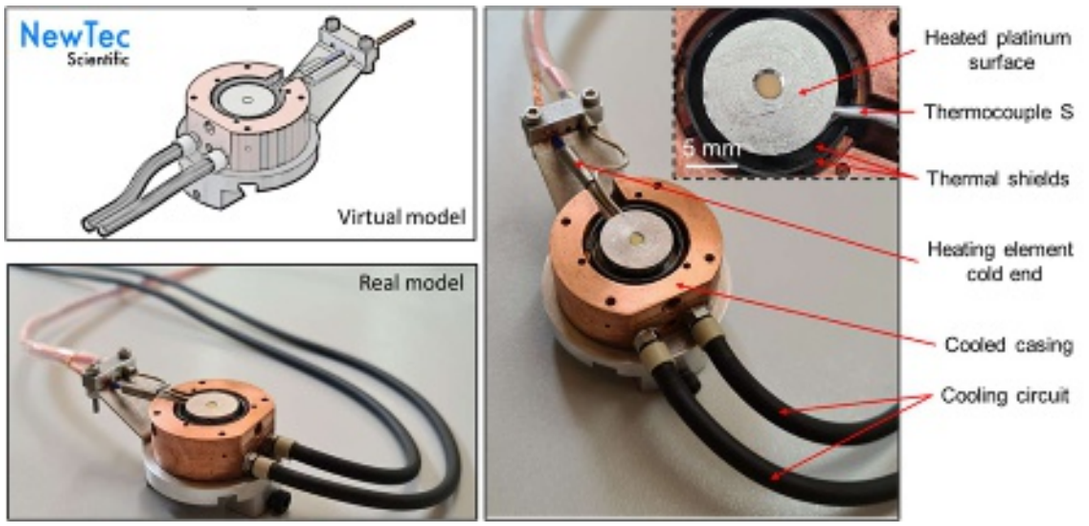

Figure 4 - Photographs of the real FurnaSEM microfurnace produced from the virtual model designed and simulated. The general appearance and dimensions of the real furnace are in line with those defined for its digital counterpart.

3.1. Creating a dedicated test bench

In order to analyze the FurnaSEM microfurnace's behavior under real-life conditions, a dedicated test bench was specially developed, comprising various components to reproduce vacuum conditions typical of those encountered in an environmental SEM. The working volume is a 6-liter chamber where the FurnaSEM device is installed for testing. **Figure 5a** shows the various components of this test bench. The chamber is evacuated using a primary dry diaphragm pump (PFEIFFER Vacuum) to achieve a limiting pressure of 100 Pa, and a turbo-molecular pump (PFEIFFER Vacuum) to achieve a high vacuum of between 10^{-3} and 10^{-4} Pa. Two pressure gauges (PFEIFFER Vacuum) are mounted close to the chamber, a Pirani-type gauge capable of measuring pressure between 10^{-2} and 10^{5} Pa, and a full-range gauge (Pirani and Penning) capable of measuring pressure between 10^{-7} and 10^{5} Pa.

Thermography is used to record the surface temperature field of the FurnaSEM microfurnace. The thermal camera used is a PI1M model (OPTRIS GmbH) featuring a 382×288 pixels CMOS detector sensitive to a narrow spectral band in the near infrared (IR) (0.85 - 1.1 µm). The measurement range for a blackbody target is between 450 and 1800°C. A fused silica window (Edmund OPTICS) allows thermal radiation from the furnace to be transmitted. Precision thermography requires an accurate description of the thermal scene in the working volume, in order to reproduce the actual temperature at the surface of the device (**Figure 5b**). A fully detailed assessment of the physical factors to be taken into account is described in supplementary information **SI-2**. This evaluation allows us to determine that a correction is necessary to estimate the furnace temperature. This correction takes into account

the emissivity of the furnace and the transmittance of the enclosure's sealed window. The equation representing this correction is given by:

$$L^0_{0.85-1.1\mu m}(T) = \frac{L^{camera}}{\tau^{window}_{0.85-1.1\mu m} \times \varepsilon^{FurnaSEM}_{0.85-1.1\mu m}} \quad (3)$$

Where $L^0_{0.85-1.1\mu m}(T)$ is the furnace blackbody radiance power used to deduce temperature, L^{camera} is the radiance power detected by the camera, $\tau^{window}_{0.85-1.1\mu m}$is the window transmittance over the spectral band of interest and $\varepsilon^{FurnaSEM}_{0.85-1.1\mu m}$is FurnaSEM's emissivity over the spectral band of interest. Measurement accuracy is directly impacted by knowledge of these parameters. According to the window characteristics supplied by EDMUND OPTICS and literature data on material emissivity [51,55] these parameters are evaluated at:

- $\varepsilon_{0.85-1.1\mu m} = 0.25 \pm 0.05$ (Platinum hot surface)
- $\varepsilon_{0.85-1.1\mu m} = 0.265 \pm 0.085$ (Magnesia insulating screw)
- $\tau_{0.85-1.1\mu m} = 0.925 \pm 0.025$ (Fused silica window)

The sensitivity of temperature measurements to these parameters has been rigorously studied and is described in the supplementary information file **SI-2**. It has been established that temperature measurements taken with the thermal camera are reliable to within 3 - 4%.

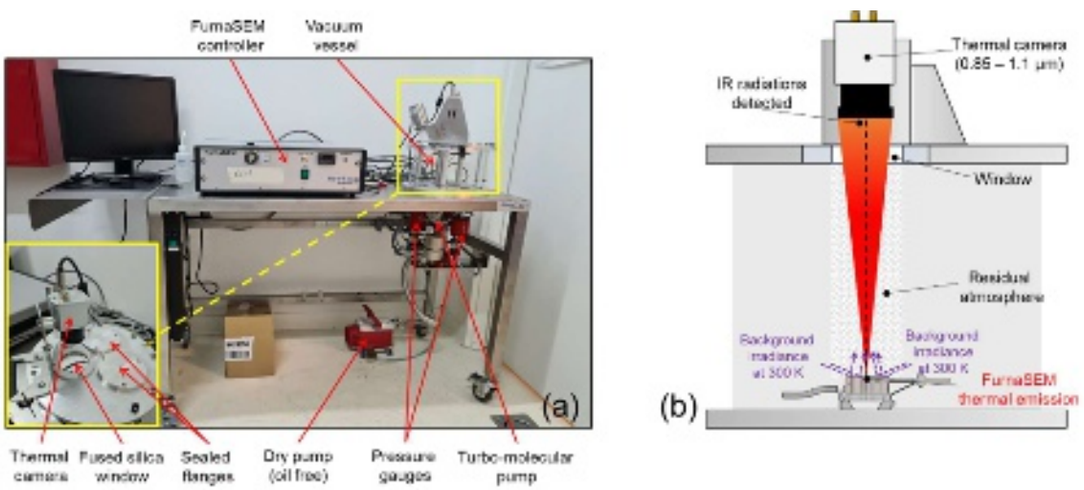

Figure 5 - Test bench developed to qualify the performance of the FurnaSEM microfurnace in an environment close to that encountered in a SEM chamber. (a) Photographs of the installation with all the equipment. (b) Thermal scene on which IR thermographs are acquired with a thermal camera.

3.2. Controlled heat treatments

The tests carried out to evaluate FurnaSEM's performances consist of controlled temperature cycles in high vacuum (10^{-3} Pa) or low vacuum (100 – 300 Pa) mode. Heating

power, local furnace temperature and IR thermography are continuously recorded during these tests. The furnace is controlled by a PID controller, which enables a thermal cycle to be programmed in a succession of steps, where the heating ramp and setpoint temperature are implemented. The heating rate is limited by the maximum permissible power of 50 W and by the thermal shock resistance of the furnace components. Studies carried out in the design phase theoretically make heating ramps of up to 10°C/s possible. Cooling control is less straightforward. To cool the FurnaSEM microfurnace, an active on-off cooling circuit without flow control is used. A controlled cooling ramp can only be achieved up to a threshold temperature called the "break point", below which cooling can no longer be controlled. This non-controllable cooling mode is referred to as " natural cooling ", as its kinetics are determined by the total intensity of heat leakage from the system. This threshold temperature depends on the desired cooling rate and the level of residual gas pressure in the test bench.

3.3. Steady-state performance

Several temperature stages were carried out over the 20 – 1300°C temperature range to determine the actual characteristics of the FurnaSEM microfurnace at thermal equilibrium. These measurements were carried out at two pressure levels (10^{-3} Pa and 300 Pa air). Typical data obtained for HV and LV conditions are shown in **Figure 6**.

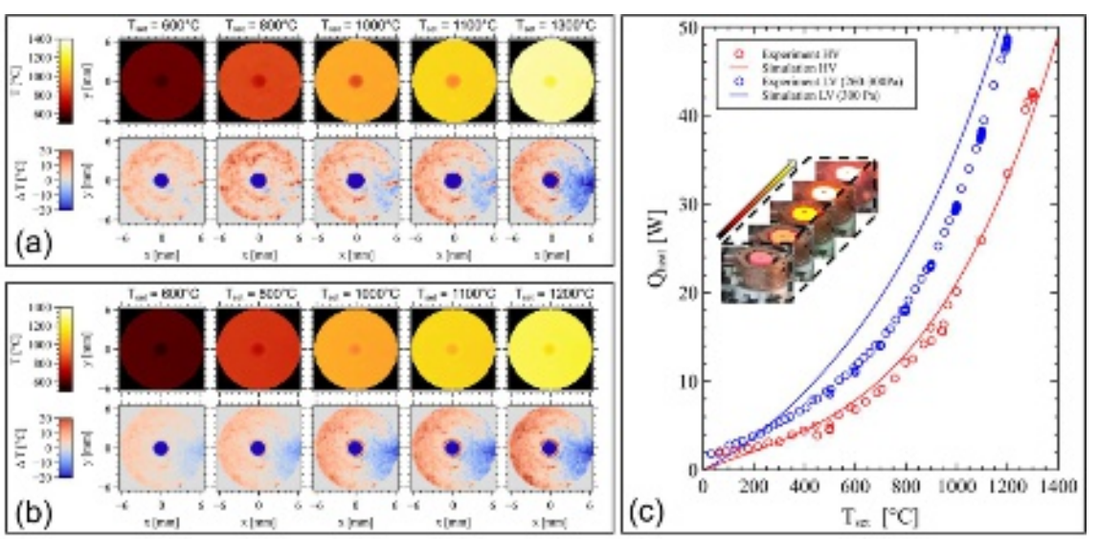

Figure 6 - Real FurnaSEM microfurnace performances recorded in steady state. (a) Heat maps and thermal fluctuations maps in high vacuum mode. (b) Heat maps and thermal fluctuations maps low vacuum mode. (c) Resulting heating power-temperature curves. Previous curves from simulations are shown as solid lines.

Thermographic reconstruction of the temperature field at the furnace surface shows that the experimental data are in good agreement with the heat maps obtained by simulation.

In particular, the distribution of hot-cold disparities is very similar in both maps. Cooler regions are located on the thermocouple side. The experimental power-temperature curves also show a similar pattern to the numerical predictions. The experimental data recorded in high-vacuum mode are well described by the numerical model (**Figure 6c**). However significant discrepancies are observed between experimental data recorded in low-vacuum mode and the results of numerical simulations. Under these conditions, the numerical simulations overestimate convective heat loss to the ambient air. This difference can be attributed to the fluid model used by the software, which is not optimized to accurately reproduce the actual experimental situation. The continuous medium assumption imposed by the numerical simulations is not sufficiently robust under these conditions, as the mean free path of air molecules at 300 Pa in the working chamber is too large to verify this assumption (see **SI-1** for a detailed discussion about the model accuracy at low pressure conditions). At present, the numerical model used for this study cannot accurately account for heat transfer in low-vacuum mode.

3.4. Rapid transient heating and cooling performance

The behavior of the furnace was also studied in detail during unsteady phases, in order to verify the performance limits of the system. In particular, heat treatments with high heating and cooling rates were implemented. Given the controller's capabilities and the temperature limits of the sensitive elements, a maximum heating ramp of 7°C/s was achieved in both high vacuum mode (up to 1300°C) and low vacuum mode (up to 1200°C). The thermal imaging camera, which acquires data at a rate of 27 Hz, was used to monitor heat propagation during this fast-heating ramp. Heat diffusion is plotted in **Figure 7**, where a temperature threshold set at 1000°C is shown in red. Heat propagation is complex, with the hot regions identified on the heat maps being the first to reach the threshold value. The heat then spreads to cooler regions near the thermocouple, before the entire surface exceeds the threshold temperature. For a constant heating ramp of 7°C/s, it takes around 6 s for the entire surface to exceed 1000°C.

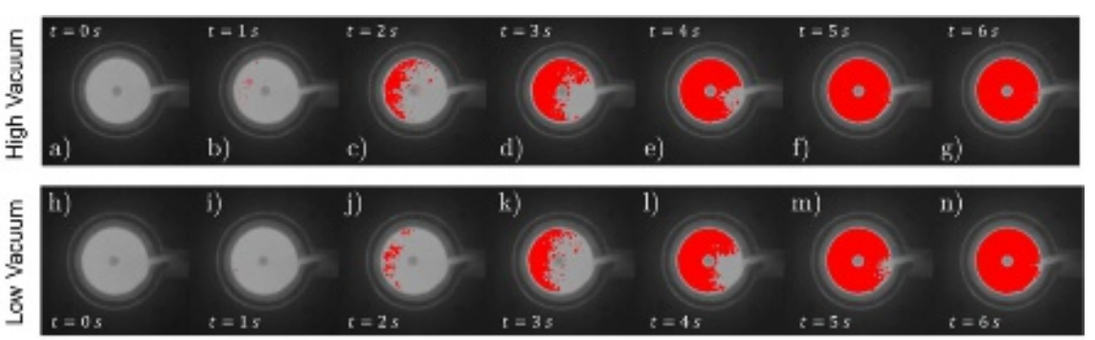

Figure 7 - Heat diffusion during temperature rise at 7°C/s. Red color = 1000°C threshold is reached. (a)-(g) Heating in high vacuum mode. (h)-(n) Heating in low vacuum mode (130 Pa air)

The maximum cooling speed is only achievable under natural cooling conditions. In this case, the cooling rate is controlled by the thermal inertia of the device and the magnitude of heat losses, taking into account all heat transfer modes. To quantify the limits of the system, the power supply to the high-temperature microfurnace was switched off. All other things being equal, the natural cooling of the furnace was recorded. By monitoring the furnace temperature, the cooling kinetics can be determined. Similar tests were repeated for varying initial temperatures, in high-vacuum or low-vacuum modes. Typical natural cooling curves are shown in **Figure 8a**. The curves shown in **Figure 8b** reflect the cooling kinetics of the furnace. In this projection, the maximum cooling rate is a function of the initial temperature of the microfurnace and the vacuum level in the chamber. The presence of residual gas pressure in the chamber accelerates microfurnace cooling when compared with recordings in high-vacuum mode. Natural cooling of the microfurnace is not linear with time, and the maximum cooling rate attainable at a given temperature varies with the furnace temperature (**Figure 8b**). For example, the maximum cooling rate is 4°C/s when the microfurnace temperature is 400°C. These measurements show that the maximum accessible cooling rate is 40°C/s for a temperature of around 1200°C, in the presence of a residual atmosphere of 300 Pa of air.

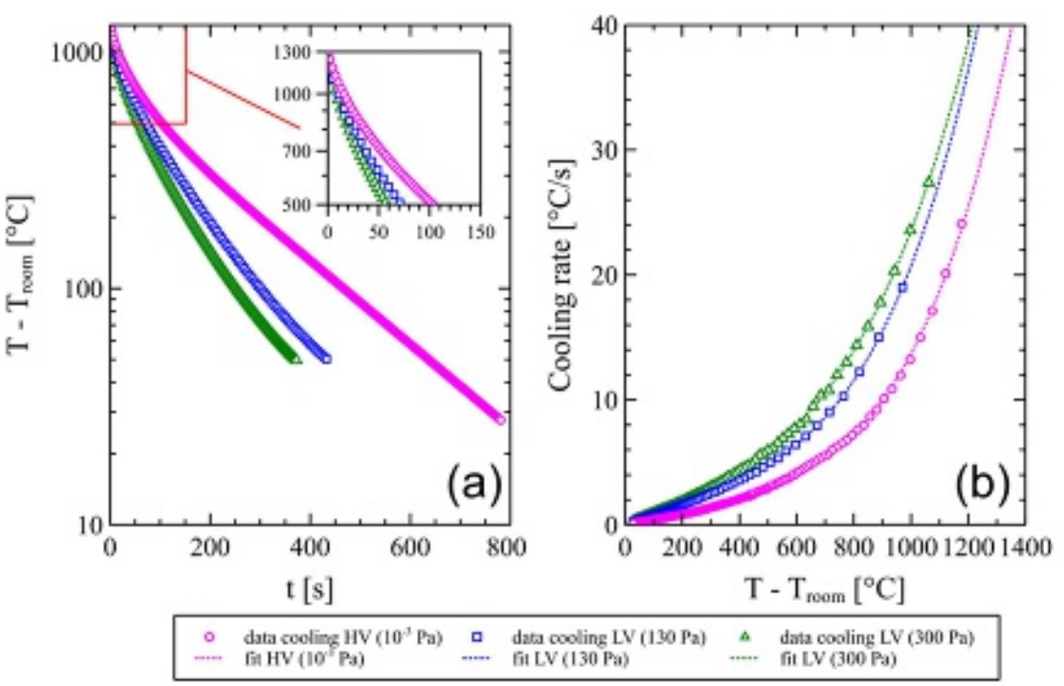

Figure 8 - FurnaSEM microfurnace natural cooling measurements recorded during tests where the power supply is switched off while the furnace is at high temperature. (a) Temperature vs. time (measurements taken at 3 different vacuum levels). (b) Equivalent natural cooling rates.

3.5. Summary of FurnaSEM microfurnace technical specifications

The results of all the tests carried out provide a summary of the furnace's technical characteristics. These characteristics vary according to the pressure level in the test bench chamber. A distinction must be made between tests carried out in high vacuum mode (HV), which enable a maximum temperature of 1300°C to be reached, and tests carried out in low vacuum mode (LV), where the maximum furnace temperature is 1200°C due to a limited power supply.

On the basis of all the tests carried out to determine FurnaSEM's performance, curves representing the furnace's operability range are constructed. These curves are shown in **Figure 9**. The operating range of the FurnaSEM microfurnace differs slightly depending on whether tests are carried out in high vacuum or low vacuum mode. In high vacuum mode, there is very little heat exchange between the microfurnace and the residual atmosphere, and convective heat loss is extremely limited. The microfurnace can be heated in a controlled manner between 20 and 1300°C, with a maximum heating rate of 7°C/s over the entire temperature range. Conversely, cooling of the microfurnace can only be controlled up to a threshold temperature ("break points" in inserts of **Figure 9**) which depends on the chosen cooling rate.

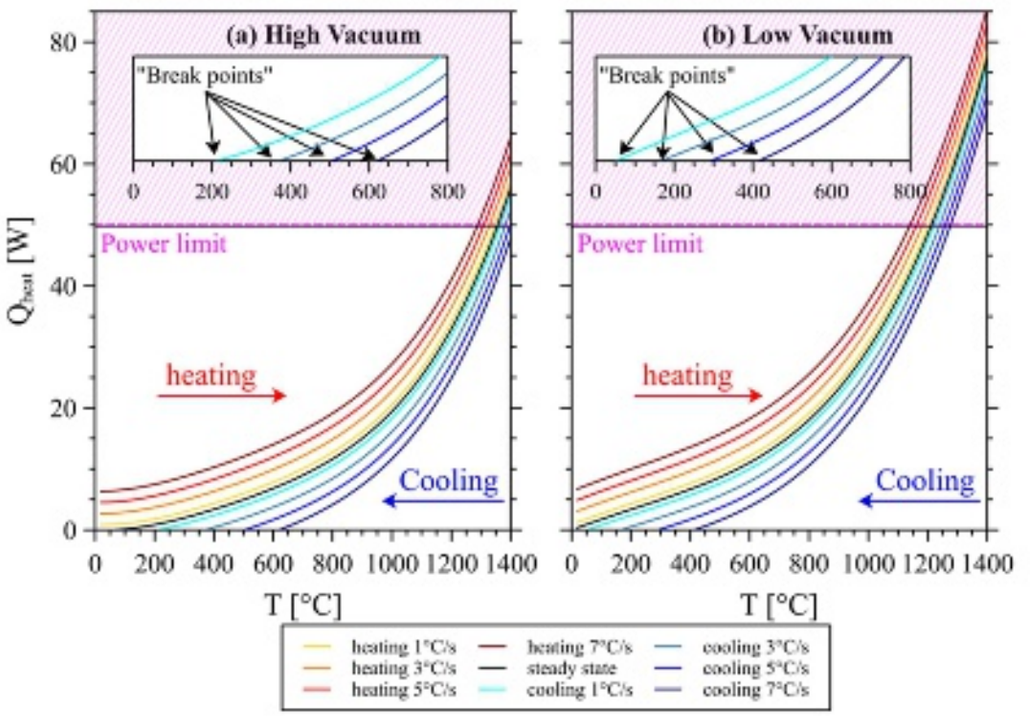

Figure 9 - FurnaSEM operability curves for the (a) high vacuum and (b) low vacuum modes used in the tests. The insets represent the "break points" corresponding to the minimum temperatures at which cooling can be controlled.

3.6. Lifetime of the FurnaSEM microfurnace

The FurnaSEM microfurnace was used to carry out measurements on the test bench and a series of *in situ* experiments in the SEM. During these experiments, high heating and cooling rates were used, with temperatures most often between 600 and 1300°C, with isothermal stages sometimes lasting up to several hours. The microfurnace was used in both high-vacuum and low-vacuum modes, with a wide variety of atmospheres (air, pure oxygen, hydrogenated nitrogen, etc.).

In the last experiment, the device was heated to 1420°C for several tens of minutes. During this experiment, the temperature of the microfurnace suddenly dropped, indicating a failure which led to the microfurnace being shut down. Diagnostics showed that the resistance of the heating wire rose sharply after the microfurnace was shut down making it unusable. Reasons of this failure are not totally clear but it is suspected that the heating element undergoes an electrical short. A Likelihood explanation can be the generation of electrical leakage induced by an electrical insulation drop of the mineral powder within the heating element. The insulation resistance decreases with temperature and may have reach a threshold point which conduct to the element failure.

All the data from these measurements and experiments are used to construct a histogram showing the operating time of the microfurnace per 100°C temperature interval (**Figure 10**) The sum of all experiments indicates that the microfurnace operated for a cumulative total of around 72 hours, of which almost 7.5 hours were at 1300°C and above (times associated with heating and cooling ramps are not included; nevertheless, they can represent around a third to a half more residence time in a temperature range). Few data on the lifetime of the heating elements in these microfurnaces are reported in the literature. A study by Zhang et al. [24] indicates maximum lifetimes of a few tens of minutes for heating elements used up to 1500°C. For the purposes of this study, the furnace lifetime was deliberately limited by conducting the experiment at a temperature above 1400°C, which corresponds to a higher temperature range than that for which the microfurnace was designed. Consequently, the 72-hour lifetime of the microfurnace is a minimum lifetime value. This value can be extended by complying with future manufacturer's instructions, which will limit the use of the microfurnace to a maximum temperature of 1300°C. The study also showed that this furnace geometry could be used to reach higher temperatures (probably 1400 - 1450°C) with limited equipment modifications and an increase in heating capacity.

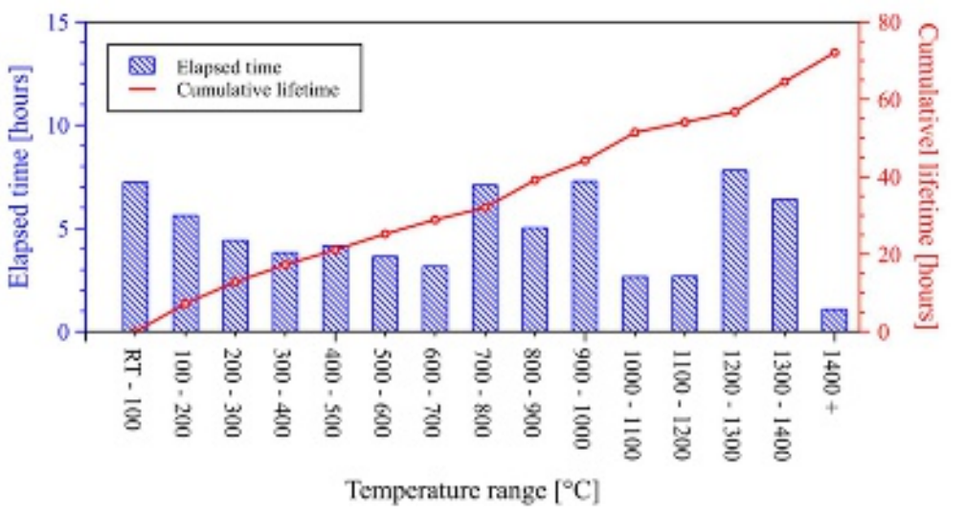

Figure 10 - Histogram summarizing FurnaSEM microfurnace time spent during heat treatment by working temperature range.

4. Conclusions

The approach adopted for this work was to develop the FurnaSEM microfurnace using a complete thermal model. After a few iterations (without building a furnace), it was possible to converge on a technical solution which is the one used for the experimental part of this study. Moreover, as the model used was developed to simulate the behavior of the hot zone of the

furnace in both high and low vacuum modes, an excellent match can be seen between the experimental data and the data obtained by numerical simulation. This a posteriori validates the approach and shows that numerical tools, if used with due regard for all the physical parameters of interest, can make a considerable contribution to the development and realization of high-performance tools.

All the experiments carried out enabled us to qualify the FurnaSEM microfurnace's behavior under conditions close to those used in the SEM chamber. On several occasions, the device reached temperatures of 1200 - 1300°C in high vacuum and low vacuum modes (up to 300 Pa). In one particular configuration, the microfurnace was heated up to 1400°C, although in this case the power supply provided by the controller was just sufficient. To reach this temperature, the addition of a heat shield covering a large part of the sample holder surface is necessary to limit the power to be supplied to the microfurnace. The lifetime of the microfurnace used in the present study is 72 hours, but this was intentionally limited to determine the maximum accessible temperature and the mode of degradation of the microfurnace.

The microfurnace can be heated to 1200°C in less than 5 minutes, with a heating ramp of 7°C/s over the entire temperature range. However, it is not possible to achieve high cooling rates (above 5°C/s) over the entire temperature range. Indeed, to cool the micro-furnace at a controlled cooling rate, the heat naturally dissipated by the furnace must be greater than the heat that needs to be dissipated at a given temperature. Below a limit temperature, natural cooling becomes limiting and controls the maximum achievable cooling rate. The maximum achievable cooling rates for each temperature have been determined.

The use of temperature maps obtained by IR thermography of the surface of interest (the area where the samples to be observed with the SEM will be positioned) enabled us to quantify the thermal gradients generated at high temperatures, and also to highlight the diffusion time when the heating rate is fast. Under all the conditions tested, the FurnaSEM microfurnace exhibited an almost uniform temperature across the entire heating surface. However, cold spots appear close to the position chosen for the thermocouple. This helps us to define a homogeneous temperature zone in which to place the sample. Excluding the cold spots, the residual temperature gradient is around ± 18°C for a temperature of 1300°C.

SUPPLEMENTARY MATERIALS

Supplementary information 01: Physical models for heat transfer simulation used in FlowSimulation©.

The physical heat transfer models used to carry out the numerical calculations and simulations are reported in detail. These models cover "Thermal conduction through solid parts", "Thermal convection with CFD model" and "Radiative heat transfer of emissive surfaces". A "Discussion about the CFD model accuracy" is also reported to show the limitations of the models used.

Supplementary information 02: Thermal scene analysis for thermography and thermal camera measurement sensibility to adjusted parameters.

The conditions for recording thermal images of the microfurnace surface using a test bench are developed in the form of a thermal scene. The "Radiation pathway to the thermal camera", and in particular the associated mathematical laws, are recalled. The "Measurement sensibility to adjustable parameters" is detailed. Taking into account the "Relationship between real and black body temperature" leads to the "Temperature uncertainty assessment". The uncertainty assessment leads to an uncertainty of 3 - 4% for the temperature displayed by the thermal camera (in Celsius scale).

ACKNOWLEDGMENT

The authors would like to thank the following organisations for helping to fund all or part of this work: the Région Occitanie and FEDER (Readynov Project Call) have funded the FurnaSEM project (2018-2021). Jerome Mendonça's PhD thesis (2019-2022) was funded by the Association Nationale de la Recherche et de la Technologie (ANRT) through the Cifre program.

AUTHOR DECLARATIONS

Conflict of Interest

The authors have no conflicts to disclose.

Author Contributions

Jérôme. Mendonça : Writing – original draft (lead); Data curation (lead); Methodology (equal); Investigation (equal).

Henri-Pierre Brau : Data curation (supporting) ; Methodology (equal); Investigation (equal).

Dorian. Nogues : Data curation (supporting); Investigation (supporting).

Antoine Candeias: Funding acquisition (equal lead); Conceptualization (Equal).

Renaud. Podor: Funding acquisition (equal lead); Conceptualization (Equal); Data curation (supporting); Investigation (supporting); Writing – review & editing (lead).

DATA AVAILABILITY

The data presented in this manuscript is available from the corresponding author upon reasonable request.

5. References

[1] R. Srinivasan, B. H. Davis, Crystallization and Phase Transformation Process in Zirconia: An in situ High-Temperature X-ray Diffraction Study. J. Am. Ceram. Soc. (1992) 75[5] 1217-1222

[2] I. Daniel, P. Gillet, B. T. Poe, P. F. McMillan, In-situ high-temperature Raman spectroscopic studies of aluminosilicate liquids. Phys Chem Minerals (1995) 22 74-86

[3] A. K. Cheetham and C. F. Mellot, In Situ studies of the Sol-Gel synthesis of materials. Chem. Mater. (1997) 9 2269-2279

[4] M. B. Pomfret, R. A. Walker, J. C. Owrutsky, High-Temperature chemistry in Solid Oxide Fuel Cells: In Situ optical studies. J. Phys. Chem. Lett. (2012) 3 3053−3064 (dx.doi.org/10.1021/jz3012047)

[5] E. Lundgren, C. Zhang, L. R. Merte, M. Shipilin, S. Blomberg, U. Hejral, J. Zhou, J. Zetterberg, J. Gustafson, Novel in Situ Techniques for Studies of Model Catalysts. Acc. Chem. Res. (2017) 50 2326−2333 (DOI: 10.1021/acs.accounts.7b00281)

[6] J. Villanova, R. Daudin, P. Lhuissier, D. Jauffrès, S. Lou, C. L. Martin, S. Labouré, R. Tucoulou, G. Martinez-Criado, L. Salvo, Fast in situ 3D nanoimaging: a new tool for dynamic characterization in materials science. Materials Today (2017) 20 354-359 (http://dx.doi.org/10.1016/j.mattod.2017.06.001)

[7] W. S. Eu, W. H. Cheung, M. Valix, Design and application of a high-temperature microfurnace for an in situ X-ray diffraction study of phase transformation. J. Synchrotron Rad. (2009). 16, 842–848 (doi:10.1107/S090904950903115X)

[8] D. H. Kim, G. Ali, J.-Y. Kim, K.-B. Kim, K. Y. Chung, Real-time X-ray analytical micro-furnace technique for in situ phase formation analysis during material synthesis. Energy Storage Materials (2023) 59 102766 (https://doi.org/10.1016/j.ensm.2023.04.005)

[9] A. M. Venkatesh, D. Bouvard, P. Lhuissier, J. Villanova, C. Rajon, In-situ 3D X-ray investigation of ceramic powder sintering at the particle length-scale. Ceramics International (2024) 50[3] 4715-4728 (https://doi.org/10.1016/j.ceramint.2023.11.216)

[10] T. Zhang, Z. Pan, C. Zhang, L. Xiong, C. Yang, J. Zhang, M. Shi, Y. Wang, W. Qu, Development of a Microheater with a Large Heating Area and Low Thermal Stress in the Heating Area. Micromachines (2024) 15 130 (https://doi.org/10.3390/mi15010130)

[11] E. A. Torres, A. J. Ramírez, In situ scanning electron microscopy. Sci. Technol. Weld. Join. (2011) 16[1] 68-78 (https://doi.org/10.1179/136217110X12785889550028).

[12] B. J. Inkson, « 2 - Scanning electron microscopy (SEM) and transmission electron microscopy (TEM) for materials characterization », in Materials Characterization Using Nondestructive Evaluation (NDE) Methods, G. Hübschen, I. Altpeter, R. Tschuncky and H.-G. Herrmann, Ed., Woodhead Publishing, (2016) 17-43. (https://doi.org/10.1016/B978-0-08-100040-3.00002-X)

[13] Z. Zhang, Y. Zhou, X. Zhu, L. Fei, H. Huang, Y. Wang, Applications of ESEM on Materials Science: Recent Updates and a Look Forward. Small Methods (2020) 4[2] 1900588 (https://doi.org/10.1002/smtd.201900588).

[14] L. Froschauer, R. M. Fulrath, Direct observation of liquid-phase sintering in the system iron-copper. J. Mater. Sci. (1975) 10[12] 2146–2155 (doi: 10.1007/BF00557493)

[15] S. K. Verma, G. M. Raynaud, R. A. Rapp, Hot-stage scanning electron microscope for high-temperature in-situ oxidation studies. Oxid. Met. (1981) 15[5] 471-483 (https://doi.org/10.1007/BF00603538)

[16] G. G. E. Seward, D. J. Prior, J. Wheeler, S. Celotto, D. J. M. Halliday, R. S. Paden, M. R. Tye, High-temperature electron backscatter diffraction and scanning electron microscopy imaging techniques : In-situ investigations of dynamic processes. Scanning (2006) 24[5] 232-240 (https://doi.org/10.1002/sca.4950240503)

[17] S. Diewald, C. Feldmann, In situ observation of the melting and sintering of submicron-sized bismuth particles. Nanotechnology (2009) 20[12] 125704 (doi: 10.1088/0957-4484/20/12/125704)

[18] C. Bocker, M. Kouli, G. Völksch, C. Rüssel, New insights into the crystallization of cordierite from a stoichiometric glass by in situ high-temperature SEM. J. Mater. Sci. (2014) 49[7] 2795–2801 (http://dx.doi.org/10.1007/s10853-013-7984-3)

[19] . Farahani, G. Zijlstra, M. G. Mecozzi, V. Ocelík, J. Th. M. De Hosson, S. van der Zwaag, In Situ High-Temperature EBSD and 3D Phase Field Studies of the Austenite–Ferrite Transformation in a Medium Mn Steel. Microsc. Microanal. (2019) 25[3] 639 - 655 (https://doi.org/10.1017/S143192761900031X)

[20] R. M. Fulrath, « High temperature scanning electron microscopy », in High temperature scanning electron microscopy , University of California Press, (1972) 347-351. (https://doi.org/10.1525/9780520323230-020)

[21] G. Gregori, H. Kleebe, F. Siegelin, G. Ziegler, In situ SEM imaging at temperatures as high as 1450°C. J. Electron Microsc. (2002) 51[6] 347–352 (https://doi.org/10.1093/jmicro/51.6.347)

[22] R. Podor, N. Clavier, J. Ravaux, L. Claparède, N. Dacheux, D. Bernache-Assollant, Dynamic aspects of ceramic sintering. HT-ESEM in situ sintering of CeO_2 at T=1400°C. Journal of the European Ceramic Society (2012) 32 353-362 (https://doi.org/10.1016/j.jeurceramsoc.2011.08.032)

[23] C. Colbea, M. Plodinec, M. Willinger, J. A. van Bokhoven, L. Artiglia, Development of a compact laser-based heating stage for in situ spectroscopic characterizations. Surf Interface Anal. (2023) 1–10 (https://doi.org/10.1002/sia.7278)

[24] Y. Zhang, L. Tang, Y. Wang, J. Wang, J. Zhou, J. Lu, Y. Zhang, Z. Zhang, Development and application of a high-temperature imaging system for in-situ scanning electron microscope Materials Today Communications 38 (2024) 107782 (https://doi.org/10.1016/j.mtcomm.2023.107782)

[25] J. E. Castle, M. R. Hunt, In situ oxidation of iron and steel in the scanning electron microscope. Corros. Sci. (1976) 16[3] 137-142 (https://doi.org/10.1016/0010-938X(76)90054-8).

[26] D. Oquab et D. Monceau, In-situ SEM study of cavity growth during high temperature oxidation of β-(Ni,Pd)Al. Scr. Mater. (2001) 12[44] 2741-2746 (https://doi.org/10.1016/S1359-6462(01)00959-9)

[27] B. Schmid, N. Aas, Ø. Grong, et R. Ødegård, High-temperature oxidation of nickel and chromium studied with an in-situ environmental scanning electron microscope. Scanning (2006) 23[4] 255-266 (https://doi.org/10.1002/sca.4950230406).

[28] F. O. Méar, R. Podor, J. Lautru, S. Genty, R. Lebullenger, Effect of the process atmosphere on glass foam synthesis: A high-temperature environmental scanning electron microscopy (HT-ESEM) study. Ceram. Int. (2021) 47[18] 26042-26049 (doi: 10.1016/j.ceramint.2021.06.010)

[29] D. J. Stokes, Principles and Practice of Variable Pressure/Environmental Scanning Electron Microscopy (VP-SEM). (2008) John Wiley & Sons Inc editors 240 pages (DOI:10.1002/9780470758731)

[30] C. Gasparrini, R. Podor, D. Horlait, M. J.D. Rushton , O. Fiquet, W. E. Lee, Oxidation of UC: an in situ high temperature environmental scanning electron microscopy study. Journal of Nuclear Materials (2017) 494 127-137 (https://doi.org/10.1016/j.jnucmat.2017.07.016)

[31] Y. Arinicheva, N. Clavier, S. Neumeier, R. Podor, A. Bukaemskiy, M. Klinkenberg, G. Roth, N. Dacheux, D. Bosbach, Effect of powder morphology on sintering kinetics, microstructure and mechanical properties of monazite ceramics. Journal of the European Ceramic Society (2018) 38[1] 227-234 (https://doi.org/10.1016/j.jeurceramsoc.2017.08.008)

[32] P. Jacquet, B. Bouteille, R. Dezert, J. Lautru, R. Podor, A. Baron, J. Teisseire, J. Jupille, R. Lazzari, I. Gozhyk, Periodic arrays of diamond-shaped silver nanoparticles: from scalable fabrication by template-assisted solid-state dewetting to tunable optical properties. Advanced Functional Materials (2019) 29 1901119 (https://doi.org/10.1002/adfm.201901119)

[33] R. Podor, X. Le Goff, J. Lautru, H.P. Brau, M. Barreau, X. Carrier, J. Mendonça, D. Nogues, A. Candeias, Direct observation of the topographic changes occurring in materials during heat treatment at high temperature. Microscopy and Microanalysis (2020) 26[3] 397-402 (https://doi.org/10.1017/S1431927620001348)

[34] O. Seppälä, A. Pohjonen, J. Mendonça, V. Javaheri, R. Podor, H. Singh, J. Larkiola, In-situ SEM characterization and numerical modelling of bainite formation and impingement of a medium-

carbon, low-alloy steel. Materials & Design (2023) 230 111956 (https://doi.org/10.1016/j.matdes.2023.111956)

[35] R. Podor, G. I. Nkou Bouala, J. Ravaux, J. Lautru, N. Clavier, Working with the ESEM at high temperature. Materials Characterization (2019) 151 15-26 (https://doi.org/10.1016/j.matchar.2019.02.036)

[36] M. Nakamura, T. Isshiki, M. Tamai, et K. Nishio, Development of a new heating stage equipped thermal electron filter for scanning electron microscopy (2002) Proceeding of the 15th International Congress on Electron Microscopy Durban, South Africa. p. 17. (Corpus ID: 201694495)

[37] L. Joly-Pottuz, A. Bogner, A. Lasalle, A. Malchere, G. Thollet, S. Deville, Improvements for imaging ceramics sintering in situ in ESEM. J. Microscopy (2011) 244[1] 93-100 (https://doi.org/10.1111/j.1365-2818.2011.03512.x)

[38] S. Dushman, Thermionic Emission. Rev. Mod. Phys. (1930) 2[4] 381-476 (https://doi.org/10.1103/RevModPhys.2.381)

[39] R. Autrata, R. Hermann, M. Müller, An efficient single crystal BSE detector in SEM: Single crystal BSE detector. Scanning (1992) 14[3] 127-135 (https://doi.org/10.1002/sca.4950140302)

[40] I. M. Fielden, J. M. Rodenburg, A Technique for Real-Time, In-Situ SEM Observation of Grain Growth at Elevated Temperatures. Mater. Sci. Forum (2004) 467-470 1385-1388 (doi: 10.4028/www.scientific.net/MSF.467-470.1385)

[41] W. Joachimi, M. Hemmleb, U. Grauel, Z.-J. Wang, M. Willinger, G. Moldovan, High-Temperature BSE and EBAC Electronics for ESEM. Microsc. Microanal. (2018) 24[S1] 694-695 (https://doi.org/10.1017/S1431927618003963)

[42] R. J. F. J. van Stratum, In-situ electron backscatter diffraction at high temperature: development of a heating and a tensile stage, Master Thesis (2019) Eindhoven University of Technology. 87 pages (https://research.tue.nl/en/studentTheses/in-situ-electron-backscatter-diffraction-at-high-temperature)

[43] A. H. Foitzik, M. W. Futing, G. Hillrichs, L.-J. Herbst, In Situ Laser Heating in an Environmental Scanning Electron Microscope. Scanning (1997) 19 119-124 (https://doi.org/10.1002/sca.4950190211)

[44] D. M Kirch, A. Ziemons, T. Burlet, I. Lischewski, X. Molodova, D. A Molodov, G. Gottstein, Laser powered heating stage in a scanning electron microscope for microstructural investigations at elevated temperatures. Rev Sci Instrum. (2008) 79[4] 043902 (https://doi.org/10.1063/1.2908434)

[45] N. A. Roberts; G. A. Magel; C. D. Hartfield; T. M. Moore; J. D. Fowlkes; P. D. Rack, In situ laser processing in a scanning electron microscope. J. Vac. Sci. Technol. (2012) A 30, 041404 (https://doi.org/10.1116/1.4731254)

[46] G. Shen, L. Wang, R. Ferry, H.-k. Mao, R. J. Hemley, A portable laser heating microscope for high pressure research. Journal of Physics: Conference Series (2010) 215 012191 (doi:10.1088/1742-6596/215/1/012191)

[47] I. Sohn, R. Dippenaar, In-situ observation of crystallization and growth in high-temperature melts using the confocal laser microscope. Metall. Mater. Trans. B (2016) 47 2083–2094. (https://doi.org/10.1007/s11663-016-0675-0)

[48] ASM Handbook: Alloy Phase Diagrams. ASM International, H. Okamoto; M.E. Schlesinger; E.M. Mueller ed. (2016) 3 (https://doi.org/10.31399/asm.hb.v03.9781627081634)

[49] Y. S. Touloukian, R. W. Powell, C. Y. Ho, P. G. Klemens, Thermophysical Properties of Matter - The TPRC Data Series. Volume 1. Thermal Conductivity - Metallic Elements and Alloys. Defense Technical Information Center (1970) 1595 pp.(ADA951935)

[50] Y. S. Touloukian, E. H. Buyco, Thermophysical Properties of Matter - The TPRC Data Series. Volume 4. Specific Heat - Metallic Elements and Alloys. Defense Technical Information Center (1971) 832 pp. (ADA951938)

[51] Y. S. Touloukian, D. P. DeWitt, Thermophysical Properties of Matter - The TPRC Data Series. Volume 7. Thermal Radiative Properties - Metallic Elements and Alloys. Defense Technical Information Center (1970) 1599 pp. (ADA951941)

[52] Y. S. Touloukian, R. K. Kirby, R. E. Taylor, P. D. Desai, Thermophysical Properties of Matter - the TPRC Data Series. Volume 12. Thermal Expansion Metallic Elements and Alloys. Defense Technical Information Center (1975) 1436 pp. (ADA129115)

[53] C. B. Alcock, V. P. Itkin, et M. K. Horrigan, Vapour Pressure Equations for the Metallic Elements: 298–2500K. Can. Metall. Q. (1984) 23[3] 309-313 (https://dx.doi.org/10.1179/cmq.1984.23.3.309.

[54] J. R. Ramble, Handbook of Chemistry and Physics - 102nd Edition. (2021) CRC Press ed. ISBN: 9780367712600 (0367712601) 1550 pp. (https://hbcp.chemnetbase.com/faces/contents/ContentsSearch.xhtml;jsessionid=F2CF4B02F8925335FC5C997684E05775)

[55] Y. S. Touloukian, D. P. DeWitt, Thermophysical Properties of Matter - The TPRC Data Series. Volume 8. Thermal Radiative Properties - Nonmetallic Solids. Defense Technical Information Center (1972) 1878 pp. (ADA951942)